IEEE Access
Multidisciplinary | Rapid Review | Open Access Journal

Received 14 September 2023, accepted 6 October 2023, date of publication 13 October 2023,
date of current version 11 January 2024.

Digital Object Identifier 10.1109/ACCESS.2023.3324551

RESEARCH ARTICLE

Next-Generation Multiband Wireless Systems: A Compact CSSR-Based MIMO Dielectric Resonator Antenna Approach

HARRIS SARFRAZ[1], SHAHID KHAN[1], NASEER KHAN[1], NEELAM GOHAR[2], SYED AHSON ALI SHAH[3], (Member, IEEE), JAMAL NASIR[1], AND MARIANA DALARSSON[4], (Senior Member, IEEE)

[1]Department of Electrical and Computer Engineering, COMSATS University Islamabad, Abbottabad Campus, Abbottabad 22060, Pakistan
[2]Department of Computer Science, Shaheed Benazir Bhutto Women University, Peshawar 25000, Pakistan
[3]Graduate School of Energy Convergence, Gwangju Institute of Science and Technology, Gwangju 61005, South Korea
[4]School of Electrical Engineering and Computer Science, KTH Royal Institute of Technology, 100 44 Stockholm, Sweden

Corresponding authors: Mariana Dalarsson (mardal@kth.se) and Shahid Khan (shahid@cuiatd.edu.pk)

This work was supported by the Swedish National Research Council under Project 2018-05001.

ABSTRACT This paper presents a compact penta-band Multiple Input Multiple Output (MIMO) Dielectric Resonator Antenna (DRA). The proposed MIMO DRA consists of two rectangular DRs incorporating complementary split ring resonators (CSRRs) and an inverted T-shaped slot. The MIMO DRA achieves low impedance matching through simple microstrip feedlines, which is further enhanced by integrating a microstrip line with the DRA itself. Remarkably, the introduction of CSRRs enables the design to resonate at five distinct frequency bands, namely 2.8-GHz, 4.4-GHz, 5.8-GHz, 6.4-GHz, and 6.9-GHz. The simulated properties of the MIMO DRA were validated through over-the-air measurements performed on a fabricated prototype. The proposed MIMO design demonstrates impedance bandwidths of 2.09 %, 2.43 %, 2.17 %, 2.55 %, and 4.91 % at the above respective resonance frequencies. The proposed design exhibits exceptional stability in radiation pattern, featuring a noteworthy peak gain of 6.08 dBi and an efficiency of 91.35 %. Notably, the incorporation of an inverted T-shaped slot effectively enhances isolation between the MIMO elements, achieving a maximum diversity gain of 10 dB and an envelope correlation coefficient of 0.005 over 20-dB isolation. A good agreement between the simulation and measured results is obtained, which underscores the suitability of the CSRR-based MIMO DRA for multiband wireless applications (blue tooth, radio astronomy, remote sensing, WIFI, satellite television and 6G), making it a very valuable contribution to the field.

INDEX TERMS DRA, CSSR, envelope correlation coefficient, ECC, diversity gain.

I. INTRODUCTION

The wireless technologies are currently experiencing an exponential growth which requires wireless nodes for Internet-of-Things (IoT) and other applications. Therefore, there is an increasing demand for compact, multiband, and high-performance antennas [1], [2] for smart devices operating at multiple frequencies, where multiband Microstrip patch antennas (MPAs) are commonly employed [3]. However, MPAs typically exhibit narrowband response, low gain, low efficiency, and limited feeding options [3]. On the other hand, Dielectric Resonator Antennas (DRAs) with their dielectric material composition offer wideband response, high efficiency, and negligible conductor losses [4], [5], [6]. Due to their three-dimensional (3D) structure, DRAs allow multiple feeding options [7], [8], [9]. In the literature there are several reports on single input single output (SISO) designs [10], [11]. However, the techniques used for multiband generation in SISO designs, such as DR deformation, defected ground structure and metamaterial

The associate editor coordinating the review of this manuscript and approving it for publication was Tao Zhou.

utilization [12], [13], suffer from low data rates, multipath fading etc. [14], [15].

The growth of wireless technologies has necessitated the utilization of MIMO DRAs, due to their ability to provide high data rates, enhanced channel capacity, and improved signal reliability [16], [17]. However, these MIMO DRAs exhibit limitations such as restricted operating bands, cumbersome size, and insufficient isolation [18]. The existing literature presents only a handful of MIMO DRAs and associated techniques that effectively address these critical issues [19], [20], [21], [22]. Notably, these techniques involve the deformation of DR shapes, deflection of the ground plane, or the adoption of hybrid structures [23], [24], [25]. While these techniques demonstrate favorable outcomes, they are accompanied by complexities and potential performance degradation [26], [27].

Consequently, numerous strategies to accomplish the realization of multiband MIMO DRAs are explored. In [28], a compact back-to-back four-port MIMO antenna system, specifically designed for LTE applications, is proposed. Their antenna incorporates an L-shaped aperture coupling feeding mechanism, utilizing an L-shaped monopole feeding structure and a slot aperture. This configuration enables multiband operations at 1.8 GHz, 2.6 GHz, and 3.6 GHz, with corresponding gains of 5.5 dBi, 5.9 dBi, and 6.9 dBi, respectively. However, the proposed design is bulkier and intricate configuration restricts its suitability for real-time applications. Similarly, in [29], a MIMO DRA design for ultra-wideband applications is proposed. Such a design incorporates two cross-shaped parasitic strips on the DRAs, excited by quadrature wave transformer microstrip feedlines. This configuration achieves resonance frequencies at 4.4 GHz, 8.3 GHz, and 10.8 GHz, with a peak gain of 5.7 dBi and a peak radiation efficiency of 96.6 %. However, the design's overall geometry remains complex, posing challenges in the fabrication process. In [26], a dual-band MIMO DRA, for mm-Wave applications, is explored. This design integrates two rectangular DRAs, each excited by a CPW feedline with etched slots in a dedicated metal ground plane. The antenna resonates at 28 GHz and 38 GHz, with minimized coupling between ports through modified CPW feed lines. Mutual coupling is enhanced by placing the DRAs with opposite orientation. However, the compactness of this design comes with complex geometry, which may present challenges in fabrication. In another study [30], a 4-port MIMO DRA is developed for WLAN and WiMAX applications, operating at 5.0 GHz and 3.5 GHz. Their proposed antenna has a ring-shaped architecture, fed by a Z-shaped aperture along with a modified microstrip line. However, the antenna geometry, with its large dimensions (80 mm $\times$ 80 mm), poses challenges in the fabrication process. In [31], a multiband MIMO DRA for LTE applications is introduced. Such an antenna operates at 0.9 GHz, 1.8 GHz, and 2.3 GHz, using a hybrid technique that combines a meander line with RDRA. While this design yields a peak gain of 3.7 dBi and a radiation efficiency of 80 %, the presence of meander lines introduces complexity and impacts the overall gain and efficiency. The antenna measures 90 mm $\times$ 107.8 mm. Furthermore, in [32] a dual-band MIMO DRA optimized for sub-6 GHz wireless applications is presented. The proposed antenna resonates at 3.5 GHz and 5.5 GHz and consists of two Ring-DRAs placed on an RT Duroid substrate. With a size of 110 mm $\times$ 50 mm, the antenna achieves a peak gain of 6.8 dBi. It should be noted that this design operates in two frequency bands and has a relatively large size. In [33], a hybrid MIMO DRA with dual-band operation is proposed. This is achieved through the use of a modified annular ring and cylindrical DRA. Such a design offers a commendable isolation of 20 dB, but with a bulky size and intricate complexity. Similarly, in [34], a triband hybrid MIMO DRA is proposed, enabling multiband operation by combining a circular ring, T-shaped line, and cylindrical DRA. Although the design demonstrates good isolation and multiband capabilities, its effectiveness is compromised due to the complex technique employed and the resulting bulky DRA. In [35], an approach is presented, introducing a DRA with a meander line for achieving multiband operations. The design exhibits a wide impedance bandwidth, enabling multiband functionality. However, due to its hybrid nature, the design suffers from low gain and backward radiation.

Another technique employed to achieve multiband MIMO DRAs is the utilization of multiple DRAs with different permittivities, as discussed in [36]. The proposed design incorporates two DRAs with permittivities of 10 and 30, resulting in two distinct bands at 3.6 GHz and 5.2 GHz, respectively, with a gain of 5 dBi. It is important to note that this technique introduces design complexity and increases the overall size of the DRA. In [37] authors achieved a mutual coupling reduction in MIMO antenna system by incorporating a T-slot, which acts as an impedance transformer of the slot formed by the edges of two PIFAs. The aforementioned MIMO systems, although innovative, face limitations such as limited operating bands, bulky size, and design complexity. Therefore, it is crucial to develop techniques that can facilitate the creation of simple, compact, and high-performance MIMO DRAs with multiband capabilities.

In the present paper we present a novel technique for achieving a multiband MIMO DRA that offers several noteworthy contributions. Specifically, we utilize a CSSR in conjunction with the DR to generate multiple operating bands. To the best of authors knowledge, a CSSR is used for the first time with the DR for the realization of five distinct operating bands, including 2.8 GHz, 4.4 GHz, 5.8 GHz, 6.4 GHz, and 6.9 GHz. To ensure improved impedance matching, a strip line is integrated with the DR, while an air gap between the DR and substrate further enhances the impedance matching performance. Moreover, the design is extended to MIMO to enhance the data rate and mitigate multipath fading. To reduce mutual coupling between the ports, an inverted T-shaped slot such as the one reported

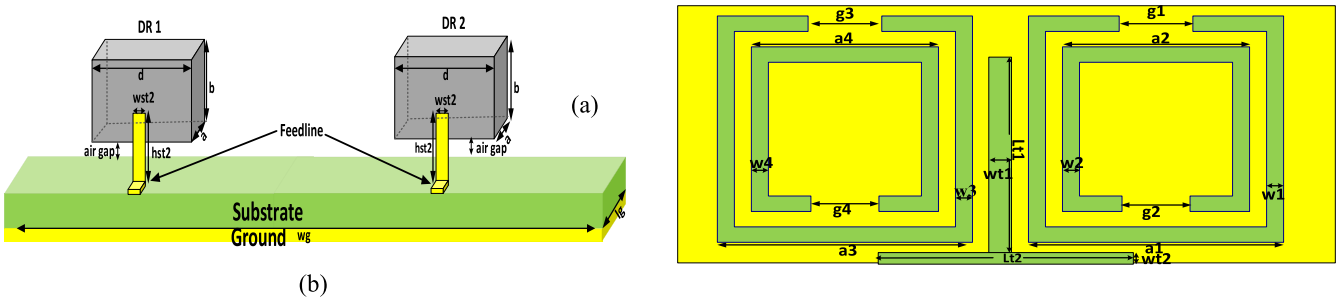

FIGURE 1. (a) Front view of design (b) Bottom view of proposed design.

TABLE 1. Detail of all dimensions of the proposed design.

Sr. No	Dimension	Value
1	a	10mm
2	b	5mm
3	d	5mm
4	ϵ_r	4.4
5	$a_{1,3}$	32.5mm
6	$a_{2,4}$	29.75mm
7	$w_{1,3}$	0.35mm
8	$w_{2,4}$	0.4mm
9	$g_{1,3}$	15.778mm
10	$g_{2,4}$	10mm
11	L_{t1}	23mm
12	L_{t2}	30mm
13	w_{t1}	1.5mm
14	w_{t2}	2mm

in [37] is introduced, thus improving isolation performance. The proposed MIMO design presents impedance bandwidths at the above respective resonance frequencies, with values of 2.09 %, 2.43 %, 2.17 %, 2.55 %, and 4.91 %. The design shows exceptional radiation pattern stability, characterized by a peak gain of 6.08 dBi and an efficiency of 91.35 %. A maximum diversity gain of 10 dB and an envelope simulation and measurement results which confirms the suitability of the CSRR-based MIMO DRA for multiband wireless applications. The main contributions of this work can be summarized as follows:

- The integration of a DR with CSSR, enabling a compact and multiband design.
- The achievement of five operating bands with a compact size, while maintaining high performance.
- The introduction of a novel decoupling technique to enhance port isolation.

The rest of the paper is organized as follows: Section II discusses the mathematical model of the proposed design. Section III discusses the parametric study of the proposed design. Section IV discusses the simulated and measured results. Section V gives details of the MIMO design and Section VI concludes the paper.

II. DESIGN AND METHODOLOGY

A. ANTENNA CONFIGURATION

The proposed MIMO DRA incorporates two rectangular DRs positioned on the top surface of the substrate, as illustrated in Fig. 1 (a) and (b). These DRs possess similar dimensions, specifically characterized by the parameters a, b, and d. They are strategically located above the substrate with dimensions Lg and Wd, while being accompanied by microstrip lines of height hst2, attached to each DR. It is important to note that both DRs feature a 1mm air gap. On the underside of the design, two CSSRs with a length of a are positioned beneath each DR. These CSSRs consist of two split rings with a defined gap denoted as g. Furthermore, the proposed design ensures port isolation through the incorporation of an inverted T-shaped slot. The excitation of the MIMO

DRA is accomplished by utilizing simple microstrip feedlines. The utilization of rectangular DRs allows for efficient utilization of the available substrate area while maintaining a compact design. The rectangular shape offers a good compromise between size and performance, enabling the accommodation of multiple resonant frequencies within a limited space. The inclusion of microstrip lines facilitates effective coupling with the DRs, ensuring efficient energy transfer and impedance matching. This arrangement helps in achieving optimal performance and reducing losses. The introduction of an air gap between the DRs and the substrate is a deliberate choice to enhance performance. The air gap acts as a dielectric discontinuity, reducing parasitic effects and improving the overall radiation characteristics of the antenna. This design consideration contributes to increased efficiency and improved radiation pattern stability. The incorporation of CSSRs beneath the DRs serves a crucial role in achieving multiband operation. CSSRs are known for their ability to exhibit resonance at multiple frequencies. By carefully selecting the dimensions and positions of the CSSRs, the proposed design achieves five distinct operating bands, enabling compatibility with a wide range of wireless applications. To ensure effective isolation between the MIMO elements, an inverted T-shaped slot is introduced. This innovative decoupling technique minimizes mutual coupling and maximizes the independence of each port, enhancing the performance of the MIMO system. It enables simultaneous transmission and reception with reduced interference, resulting in enhanced data rates and reduced multipath fading effects. The choice of simple microstrip feedlines for exciting the MIMO DRA contributes to ease of implementation and practicality. Microstrip feedlines are widely used in antenna designs due to their simplicity, low cost, and compatibility with various fabrication processes. The summary of parameters is given in Table 1.

B. DESIGN EQUATIONS

The proposed MIMO DRA design combines two key components: the design of the rectangular DRs and the design of the CSSR. Both of these components are based on mathematical principles and equations, which provide a solid foundation for their behavioral structure. The dimensions of the single-element DRA are determined based on fundamental equations [34]. The resonance frequency (f_r) of the DRA is calculated using the following equation:

$$f_r = \frac{\sqrt{k_x^2 + k_y^2 + k_z^2}}{\left(2\pi\sqrt{\mu_0 \varepsilon_0 \varepsilon_r}\right)} \tag{1}$$

Here,

$$\sqrt{k_x^2 + k_y^2 + k_z^2} = \varepsilon_r k_0^2 \tag{2}$$

where k_x, k_y, and k_z are the wave vector components in each plane, as described by equations (3)-(5). The parameter ε_r represents the relative permittivity of the material, while μ_0 signifies the permeability of the DR [3].

$$k_x^2 = \left(\frac{m\pi}{a}\right)^2 \tag{3}$$

$$k_y^2 = \left(\frac{n\pi}{b}\right)^2 \tag{4}$$

$$k_z^2 = \left(\frac{p\pi}{d}\right)^2 \tag{5}$$

where integers m, n, and p represent wave numbers across the respective dimensions of the DR (a, b, and d). The CSSR, another important component of this design, operates based on equations (6)-(13), which describe its behavioral structure. The CSSR unit cell behaves as an LC circuit with a resonance frequency (f_o) defined by equation (6) [26]:

$$f_o = \frac{1}{2\pi\sqrt{LC}} \tag{6}$$

In equation (6) L and C are the total inductance and capacitance of the CSSR which are calculated with the help of equations (7)-(12).

$$L = l\left(2.303\log_{10}\left(\frac{4l-\gamma}{w}\right)\right)2\times 10^{-4} \tag{7}$$

For the CSSR square geometry, the parameter γ =2.853 is a constant, and l is the length of CSSR which is computed as follows:

$$l = 4a - g \tag{8}$$

where a denotes the area of the CSRR unit cell and g represents the CSRR split ring gap. The total capacitance C is given by equation (9):

$$C = \frac{C_s + C_g}{2} \tag{9}$$

Here, C_s and C_g represent the series and gap capacitances of the CSSR unit cell, respectively. The gap capacitance C_g is calculated using equation (10):

$$C_g = \frac{\varepsilon_0 wt}{g} \tag{10}$$

while the series capacitance C_s is determined by equation (11):

$$C_s = C_{pul}\,(4a_e - g) \tag{11}$$

The width w and thickness t of the metal ring, as well as the free space permittivity (ε_0), are incorporated into the calculations. The per unit length capacitance C_{pul} is evaluated using equation (12):

$$C_{\text{pull}} = \frac{\sqrt{\varepsilon_r}}{vZ_0} \tag{12}$$

In equation (12), v denotes the velocity of light and Z_0 signifies the characteristic impedance. By substituting the values of C_s and C_g into equation (9), the overall capacitance is obtained as follows:

$$C = \left(2a_e - \frac{g}{2}\right)C_{\text{pull}} + \frac{\varepsilon_0 wt}{2g} \tag{13}$$

These equations play a fundamental role in the initial design of the CSSR-based SISO DRA, enabling the determination of optimal dimensions and operating characteristics.

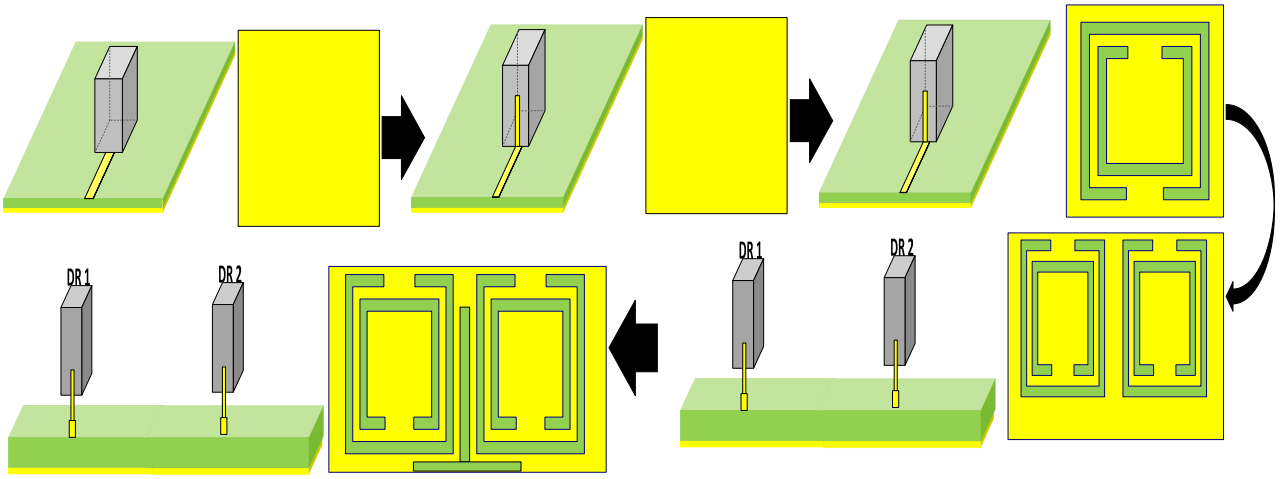

FIGURE 2. Design steps of the proposed MIMO DRA.

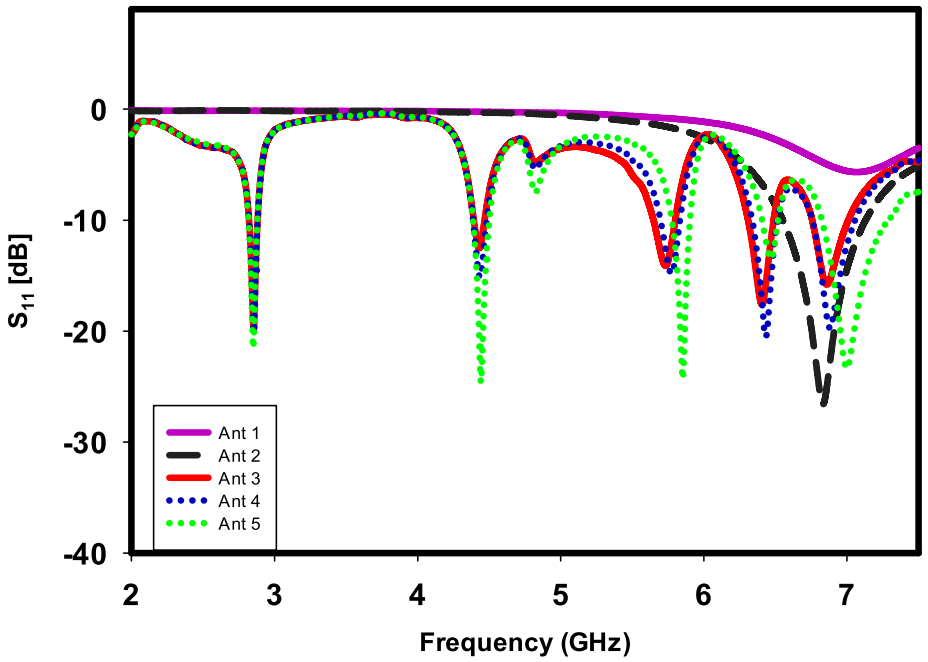

FIGURE 3. Return Loss for different design steps of the proposed design.

C. DESIGN EVALUATION

The design process of the CSSR-based MIMO DRA is illustrated in Figure 2, and the corresponding reflection coefficients are shown in Figure 3. The finalization of the design involves six steps, each contributing to the desired performance characteristics. Step 1 focuses on the initial excitation of a rectangular DR using a simple microstrip line, as depicted in Figure 2a. At this stage, the DR exhibits resonant behavior with relatively low impedance matching, as shown in Figure 3. In Step 2, the impedance matching is improved by introducing a thin stripline that extends from the feedline to the DR. This addition significantly enhances the impedance matching. To enable multiband operation, Step 3 involves the incorporation of a CSSR (Coupled Split Ring Resonator) into the ground structure. This addition of the CSSR introduces multiple resonant frequencies. However, it is observed that some of these resonance frequencies still exhibit low impedance matching. To address this issue, Step 4 introduces an air gap between the DR and the surrounding structures. This air gap enhances the impedance matching of all the resonance frequencies, resulting in improved performance across the entire frequency range. In Step 5, the design is transformed into a MIMO (Multiple-Input Multiple-Output) configuration. Due to the inherent symmetry of the MIMO arrangement, the reflection coefficients remain consistent and repetitive for each port,

as shown in Figure 3. Finally, to enhance the decoupling between the MIMO ports and further improve the isolation, Step 6 incorporates an inverted T-shaped slot between the two ports. This slot etching enhances the isolation between the ports, as demonstrated in Figure 4. It is worth noting that the introduction of the decoupling slot causes a slight right shift in the operating bands. As a result of these design steps, the finalized CSSR-based MIMO DRA exhibits multiband operation, high port isolation, and improved impedance matching.

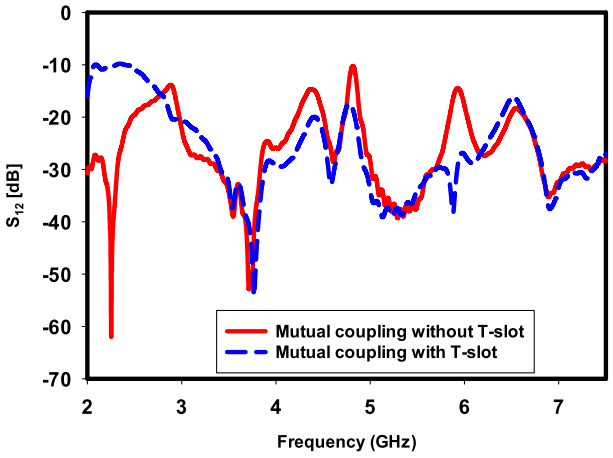

FIGURE 4. Mutual coupling comparison before and after T-slot addition.

III. PARAMETRIC STUDY

A. EFFECT ON REFLECTION COEFFICIENT

A comprehensive parametric study was conducted to investigate the impact of various key parameters in the proposed design. These parameters include the height of the DR, the height of the printed strip, and the inner and outer areas of the CSSR. Additionally, a study was conducted on the decoupling slot.

The height of the DR plays a crucial role in determining the overall compactness of the design. Figure 5 illustrates the effect of changing the DR height on the reflection coefficients. The results clearly indicate that increasing the DR height leads to a downward shift in the upper operating band. This shift aligns with the analytical equation for the DR, thereby validating its impact on the operating frequency range. Moreover, the observed trend confirms the expected behavior of the DRA. Based on the $|S_{11}|$ response and considering the available materials, a height of 5 mm is selected as the optimal value for the proposed DRA. This choice ensures a suitable balance between compactness and desirable operating frequency range.

Figure 6 presents the influence of the printed strip height on the reflection coefficients. It is evident from the figure that altering the strip line height affects both the impedance matching and the operating band. By increasing the height of the printed strip, the impedance matching is improved, resulting in better performance of the DRA. Simultaneously, the

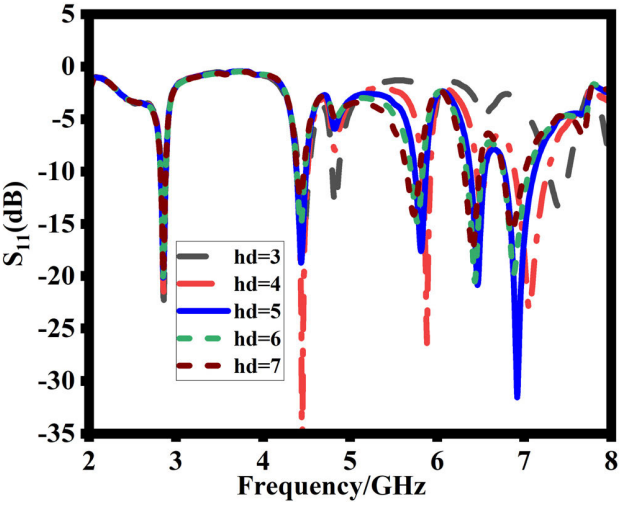

FIGURE 5. Impact of DR height on reflection coefficients.

operating band experiences a shift towards lower frequencies due to the modified electrical length introduced by the strip.

Through careful analysis, it is determined that a height of 4.5 mm for the printed strip yields the maximum number of operating bands with good impedance matching. This optimal value ensures effective coupling between the feed line and the DR, facilitating improved overall performance.

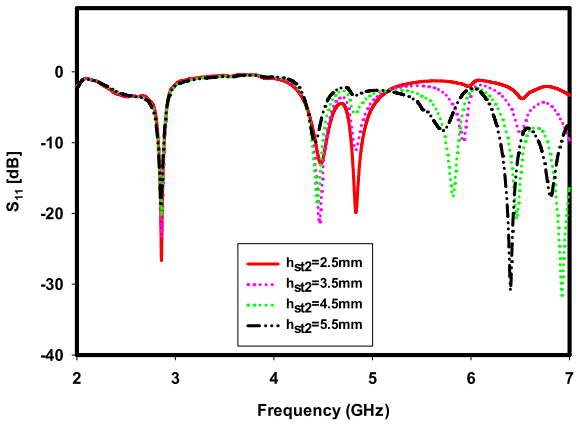

FIGURE 6. Impact of vertical strip height on reflection coefficients.

The inner and outer areas of the CSSR also significantly impact the operating band and impedance matching. Figure 7 demonstrates that increasing the length of the CSSR's inner area a_2 results in a shift of the operating band towards lower frequencies. This behavior can be attributed to the additional capacitance provided by the extended inner area, affecting the overall resonant behavior of the DRA. Based on the response of the reflection coefficients and considering the available space, a length of 29.7 mm for the inner CSSR area is chosen as the optimal value. This length allows for the desired resonance frequencies while maintaining good impedance matching throughout the operating band.

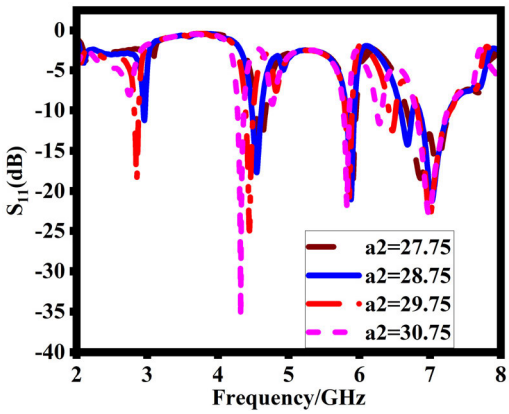

FIGURE 7. Impact of the inner area of the CSSR on the reflection coefficient.

Similarly, Figure 8 reveals that the length of the CSSR's outer area a_1 affects the impedance matching and operating band. Increasing the length of the outer CSSR area leads to a lower operating band and improved impedance matching. This effect can be attributed to the increased capacitance introduced by the extended outer area, which modifies the resonant behavior of the DRA. At a length of 32.5 mm for the CSSR, the design exhibits the maximum number of operating bands with good impedance matching. This optimal length ensures the desired multiband operation while achieving excellent impedance matching across the entire operating frequency range.

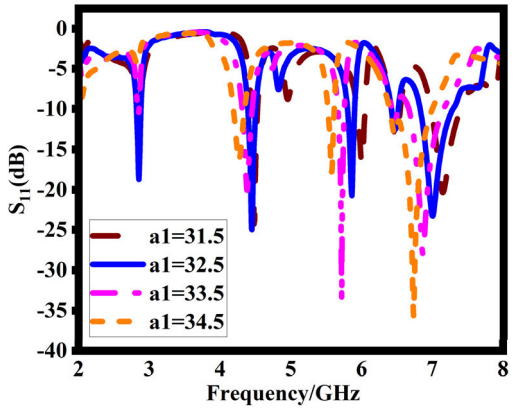

FIGURE 8. Impact of outer area on the reflection coefficients.

Through this detailed parametric study, the optimal values for the height of the DR, the height of the printed strip, and the lengths of the CSSR's inner and outer areas have been determined. These values ensure the achievement of multiple operating bands with satisfactory impedance matching, thereby enhancing the overall performance of the proposed DRA design. The insights gained from this study provide valuable guidelines for designing and optimizing similar CSSR-based MIMO DRAs, facilitating their application in various wireless communication systems.

B. ISOLATION IMPROVEMENT

To improve the isolation between the ports, an inverted T-shaped decoupling slot is incorporated into the design. The dimensions of this slot have been carefully selected based on a comprehensive parametric study. The vertical part and horizontal part of the slot are critical factors influencing the ports isolation. Figure 9 and 10 illustrate the impact of increasing the length and width of the horizontal slot on the impedance matching across the entire operating band. The results clearly indicate that as the length (lt_1) and width (Wt_1) of the horizontal slot are increased, the impedance matching is gradually enhanced. After thorough analysis, it has been determined that a horizontal slot length of 23 mm and width of 1.5 mm achieve maximum impedance matching. These dimensions ensure effective coupling between the ports, resulting in improved overall performance.

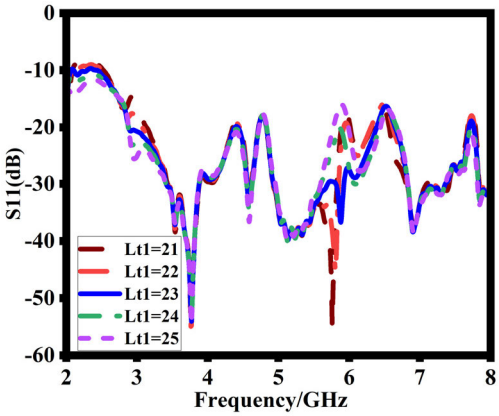

FIGURE 9. Impact of lower part of T-slot (lt1) on the reflection coefficients.

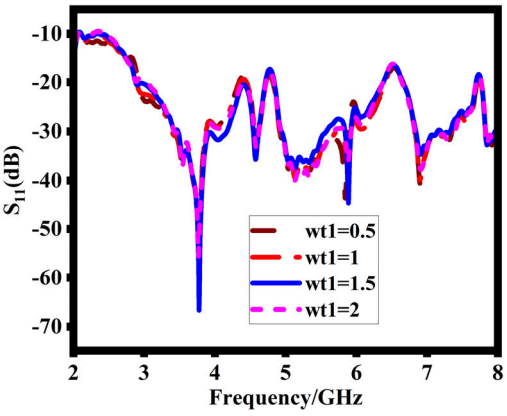

FIGURE 10. Impact of T-slot upper part (wt1) on mutual impedance.

Similarly, Figures 11 and 12 depict the effect of the vertical slot in the inverted T-shaped strip on ports isolation. By increasing the length (lt_2) and width (Wt_2) of the vertical slot, the isolation between the ports is improved. Through careful evaluation, it has been determined that a vertical slot length of 30 mm and width of 2 mm provide the

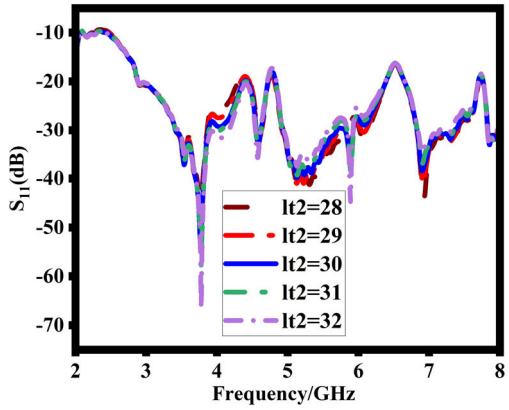

FIGURE 11. Impact of T-slot (lt2) on mutual impedance.

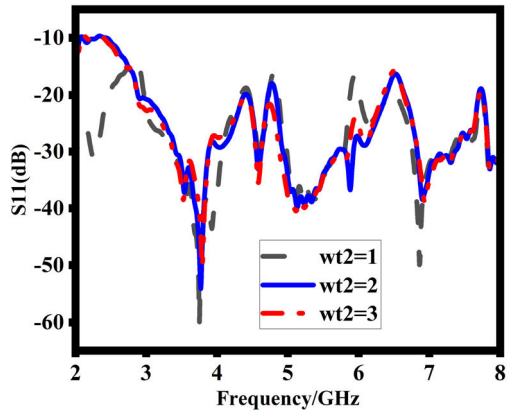

FIGURE 12. Impact of T-slot upper part (wt2) on mutual impedance.

optimal isolation between the ports. These dimensions enable effective suppression of unwanted coupling, ensuring a high level of isolation.

IV. SIMULATED AND MEASURED RESULTS

This part displays the suggested design's final simulation and measurement data, offering a thorough assessment of its performance. Reflection coefficients, mutual impedances, gain and efficiency, current distribution, and radiation patterns throughout all operating bands are among the important variables evaluated. In order to assess the degree of interference and coupling between the elements, the mutual impedances between the antenna ports are also analyzed.

A. EXPERIMENTAL SETUP

The proposed DRA and CSRR design are thoroughly modeled, simulated, and analyzed using CST Microwaves Studio software. This powerful electromagnetic simulation tool enables accurate representation and evaluation of the antenna system's performance. To validate the simulated results, the design is fabricated, and experimental measurements are conducted. An anechoic chamber, which provides an environment free from external reflections and interference, is utilized for accurate measurement of the antenna's performance. The measurements are carried out using a Vector Network Analyzer (VNA), which allows for precise characterization of the reflection coefficients, gain, and other important parameters. During the measurement process, one port of the proposed design is terminated with a 50 Ω impedance to ensure proper impedance matching and accurate measurement of the reflection coefficients by eliminating any undesired effects that may arise from open or short-circuited ports, allowing for reliable and consistent measurements.

B. SCATTERING PARAMETERS

The reflection coefficients of the proposed design are evaluated through simulation and measurement, as shown in Figure 13. Overall, there is a close agreement between the simulated and measured results, indicating the validity of the design. However, some minor discrepancies in impedance matching are observed, particularly at higher bands. This can be attributed to fabrication inaccuracies and imperfections in the measuring environment. Additionally, a slight shift in the last operating band towards higher frequencies is observed, which may be influenced by the presence of a minor air gap in the individual DRA structure. Despite these discrepancies, the general agreement between the simulated and measured reflection coefficients validates the design's performance.

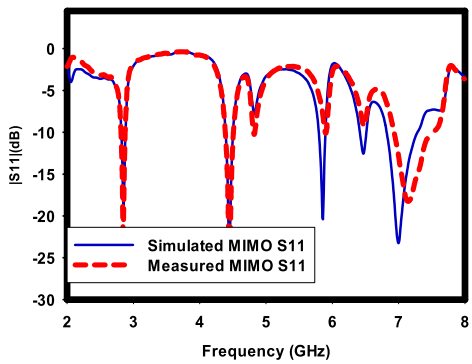

FIGURE 13. Simulated and Measured reflection coefficients of the proposed design.

Figure 14 presents the simulated and measured mutual impedance of the proposed design. The measured mutual impedance closely follows the simulated results, demonstrating the accuracy of the design model. However, at 4.5 GHz, a mismatch between the simulated and measured results is observed, which can be attributed to fabrication imperfections. It is important to note that the accurate fabrication of complex antenna structures can be challenging, leading to slight variations in performance. Nonetheless, the overall agreement between the simulated and measured mutual impedances indicates the effectiveness of the proposed design. For a comprehensive overview of the simulated and measured results, Table 2 provides detailed information on the reflection coefficients and mutual impedances at different frequencies.

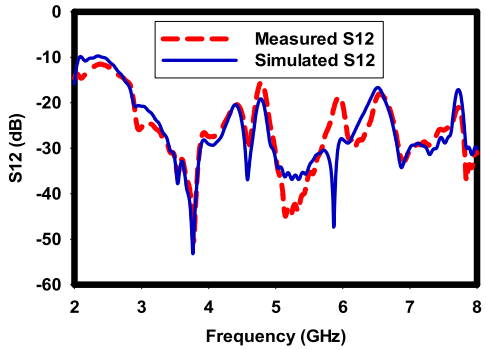

FIGURE 14. Simulated and Measured mutual impedance of the proposed design.

TABLE 2. Detail of the simulated and measured reflection coefficients.

Sr. No	Freq. (GHz)	Simulated Bandwidth	Measured Bandwidth	Simulated mutual impedance (dB)	Measured mutual impedance (dB)
1	2.85	2.8229 – 2.8827	2.8227-2.8826	-17	-16
2	4.44	4.3854 – 4.4934	4.3852-4.4935	-21	-22
3	5.81	5.6979 – 5.8339	4.7100-5.85002	-30	-32
4	6.46	6.3383 – 6.5144	6.3500-6.6114	-25	-27
5	7.02	6.7591 – 7.0565	6.9400-7.6570	-30	-32

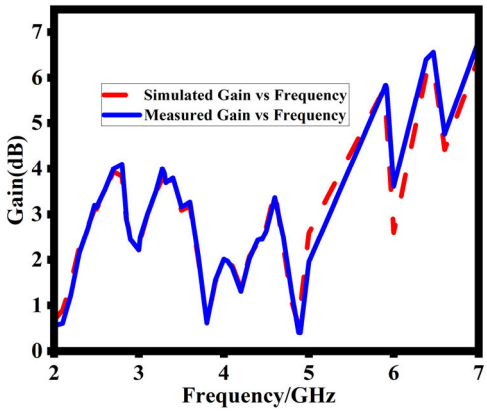

FIGURE 15. Gain of the proposed design for the multiple operating bands.

C. GAIN AND EFFICIENCY

The performance and effectiveness of an antenna's capacity to radiate and transmit power are strongly influenced by its gain and efficiency characteristics. Figure 15 shows the evaluation of the gain of the proposed design over the operating bands using simulation and measurement. Overall, the simulated gain values for the lower and higher operating bands closely agree with the measured results. At the mid-range frequencies, a minor difference between the simulated and measured results is noticed. Fabrication tolerances and measurement errors are just two reasons for this mismatch in the simulated and measured results. The broad consistency between the simulated and measured gains, despite this little variation, shows that the design is successful in providing the desired radiation properties. Table 3 summarizes the simulated and measured gain and efficiencies at all operating frequencies.

Figure 16 illustrates the efficiency of the proposed design across the entire operating band. Initially, the design exhibits high efficiency at low frequencies. However, a decline in both gain and efficiency is observed around 4 GHz and 5 GHz. This decrease in performance can be attributed to the low mutual coupling between the elements at these specific operating frequencies. The current distribution analysis confirms that there is limited current flow between the ports at these frequencies, resulting in reduced gain and efficiency. Conversely, at higher frequencies, the gain and efficiency of the design improve due to better isolation between the ports.

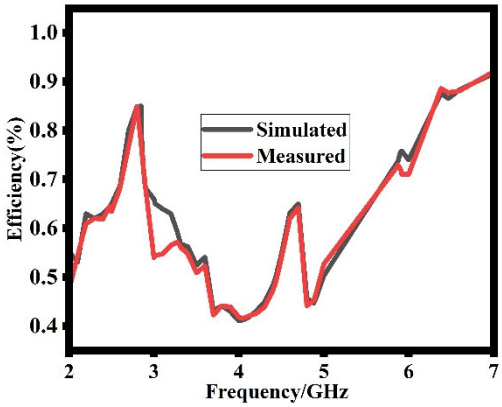

FIGURE 16. Efficiency of the proposed design over the operating bands.

D. CURRENT DISTRIBUTIONS

The current distribution within the proposed design at the target resonance frequencies provides insights into the behavior and mode of operation of the antenna. Figure 17 presents the current distribution patterns at specific frequencies. At 2.8 GHz (Figure 17(a)), the current is uniformly distributed along the inner CSSR, while it is concentrated on the lower parts of the outer CSSR. This distribution pattern indicates a balanced current flow within the design, contributing to the desired resonance at this frequency. At 4.4 GHz (Figure 17(b)), the current is uniformly distributed on both the outer and inner CSSR, with no significant activity between Port 1 and Port 2. This behavior ensures a high level of mutual coupling, enabling effective communication and transmission at this frequency. At 5.8 GHz (Figure 17(c)), the current distribution on the inner and outer CSSR is relatively reduced,

TABLE 3. Detail of the simulated and measured gain and efficiency.

Sr. No	Resonance Frequency (GHz)	Simulated Gain (dBi)	Measured Gain (dBi)	Simulated Efficiency	Measured Efficiency
1	2.85	4.0	4.01	0.85	0.86
2	4.44	2.40	2.50	0.65	0.66
3	5.81	5.90	5.95	0.75	0.77
4	6.46	6.0	6.1	.85	0.87
5	7.02	6.08	6.15	0.93	0.935

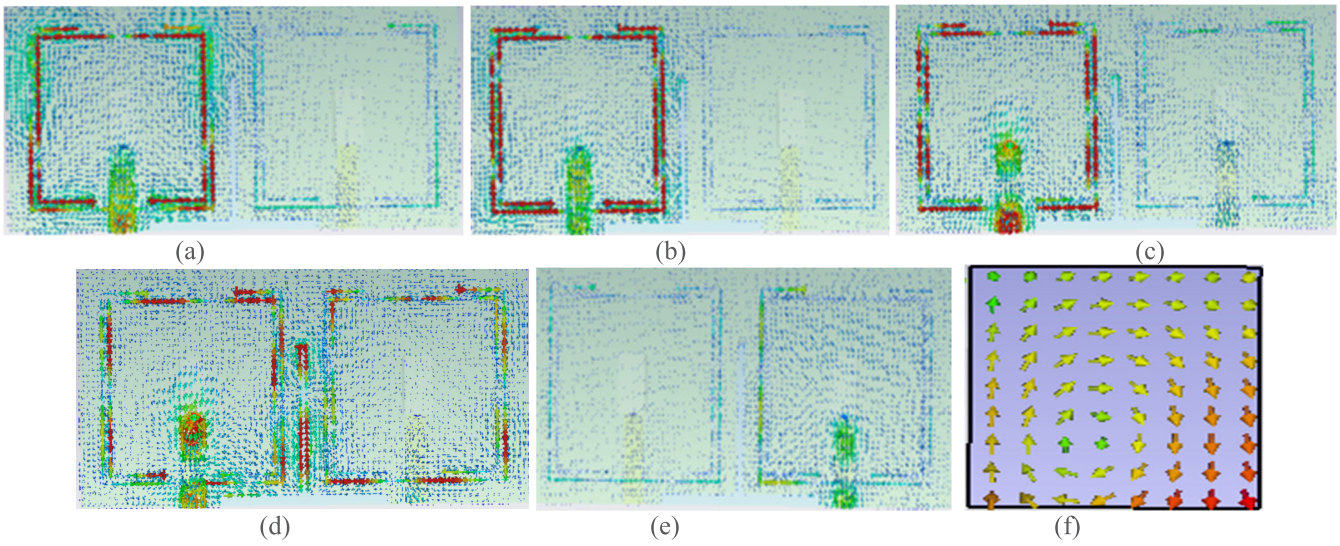

FIGURE 17. Surface current at (a) 2.8GHz (b) 4.4GHz (c) 5.8GHz (d) 6.4GHz and electric field distribution on the DR at (f) 7.04 GHz.

and a noticeable flow of current between Port 1 and Port 2 is observed. This current flow between the ports decreases the mutual impedance at 5.8 GHz, indicating a change in the mode of operation. Similarly, at 6.4 GHz (Figure 17(d)), the current distribution on the inner and outer CSSR is present, while no significant current flow is observed between the ports. This current distribution pattern maintains a higher mutual impedance at 6.4 GHz, suggesting a different resonance mode. At 7.04 GHz, no significant current activity is observed on the inner and outer CSSR, indicating that this frequency is primarily influenced by the electric field distribution within the DR. Figure 17(f) further demonstrates the electric field distribution on the top surface of the DR, revealing the operation of a TE110 mode at 7.04 GHz.

E. FAR-FIELD RADIATION PATTERN

The target resonance frequencies of the proposed design together with the electric (E) and magnetic (H) far-field radiation patterns are shown in Figure 18(a–e). By activating Port 1 and terminating Port 2 with a 50-ohm load, the radiation patterns were analyzed. Both ports simulated and measured radiation patterns show an omnidirectional nature and both are in good agreement. Every port exhibits the same radiation patterns, demonstrating uniform performance across the working bands. Peak gains for both ports range from 2 to 6.08 dBi, indicating the antenna's radiated power in various directions.

It should be emphasized that small differences between the measured and simulated radiation patterns at 7.04 GHz might be attributable to manufacturing mistakes and less-than-ideal testing conditions. These factors may cause minor changes in the antenna performance at particular frequencies. The top and bottom views of the fabricated prototype are shown in Figure 19 (a) and (b), respectively. Figure 19(c) shows the fabricated prototype set up within the measuring apparatus for measurements of the far-field radiation pattern, ensuring reliable assessment of the antenna's radiation properties.

V. MIMO PARAMETERS

In this section, important factors like the envelope correlation coefficient (ECC), diversity gain (DG), channel capacity loss (CCL) and total active reflection coefficient (TARC) are analyzed in order to evaluate the MIMO and diversity performance of the proposed antenna.

A. ENVELOPE CORRELATION COEFFICIENT

In MIMO antenna systems, the ECC is a critical parameter since it measures the correlation or isolation between the various communication branches. Equation 14 is used to

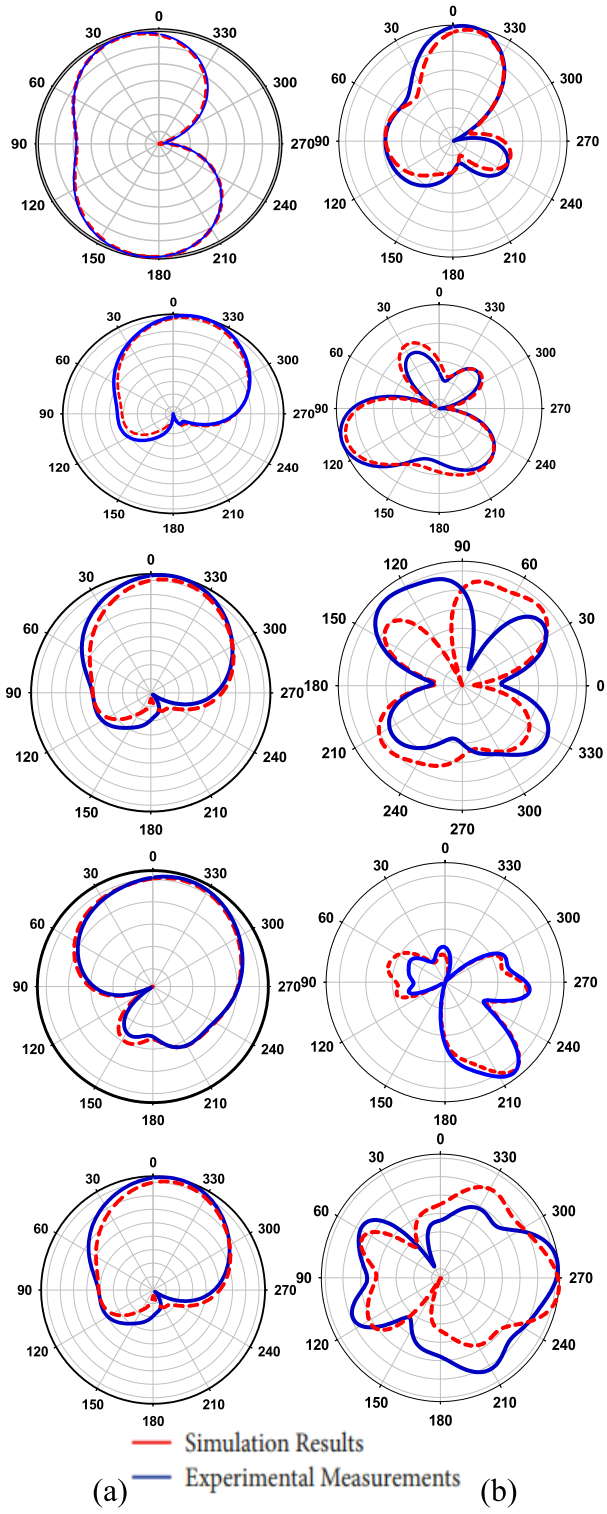

FIGURE 18. Radiation pattern (a) E-field and (b) H-field of the proposed design at 2.8GHz, 4.4GHz, 5.8GHz, 6.4GHz and 7.04GHz respectively.

represent the ECC in this work, which computes it using the S-parameters of the proposed MIMO antenna. For good MIMO performance, an ECC value less than 0.5 is often preferred [31]. The provided MIMO antenna's simulated and measured ECC is shown in Fig. 20. The findings firmly show that the ECC is still considerably below 0.1 in the targeted frequency ranges. Excellent isolation between the antenna elements is necessary for attaining high-quality MIMO communication, is indicated by the low ECC values.

$$\rho_e = \frac{|\sum_{n=1}^{N} S_{in}^* S_{nj}^* - \sum_{n=1}^{N} L_{ij}^n|^2}{\prod_{k-ij}[1 - \sum_{n=1}^{N} S_{kn}^* S_{nk} - \sum_{n=1}^{N} L_{kk}^n} \quad (14)$$

where 'i' and 'j' are two antennas in the proposed MIMO antenna system.

B. DIVERSITY GAIN (DG)

Another important variable that assesses the improvement offered by a MIMO system over a single antenna system is the diversity gain (DG). DG is calculated using Equation 15, which quantifies the improvement in signal quality achieved through diversity techniques. The simulated and measured DG of the designed MIMO antenna is illustrated in Fig. 21. The findings show that the DG is approximately 10 dB in the relevant frequency ranges. For a two-element MIMO system, this high DG value signifies outstanding MIMO performance [31]. The achieved DG highlights the effectiveness of the proposed antenna design in improving signal reliability and robustness in MIMO communication scenarios. Table 4 provides comprehensive information on the MIMO performance of the proposed antenna.

$$\mathrm{DG} = 10\sqrt{(1-\mathrm{ECC}^2)} \quad (15)$$

C. CHANNEL CAPACITY LOSS (CCL)

CCL, or channel capacity loss, is an essential MIMO metric. It refers to the reduction in the data rate due to numerous factors which include some practical limitations and imperfections, multipath loss and environmental factors. CCL reflects the efficacy of the design throughput. Good data rates are indicated by a lower CCL value. CCL is based on certain mathematical equation, which is given in equations (16)-(19):

$$C\ (Loss) = -\log_2 \det(\psi^R) \quad (16)$$

where ψ^R is the correlation matrix at the receiving antenna.

$$\psi^R = \begin{bmatrix} \rho 11 & \rho 12 \\ \rho 21 & \rho 22 \end{bmatrix} \quad (17)$$

$$\rho \mathrm{ii} = 1 - \left(|Sii|^2 + |Sij|^2\right), \quad for\ i,j = 1\ or\ 2 \quad (18)$$

$$\rho \mathrm{ii} = -(Sii * Sij + Sji * Sij), \quad for\ i,j = 1\ or\ 2 \quad (19)$$

A high correlation between the antennas elements induces loss of capacity which is explained by channel capacity loss. Thus, determination of CCL depends on the S-parameters. A good impedance matching and port isolation ensures a good CCL. A 0.4 bits/sec/Hz CCL is an indicator of good data transmission. Figure 22 describes the simulated CCL for the five operating bands. Figure 22 shows that at all operating bands, the design has values of CCL lower than 0.4 bits/sec/Hz CCL.

FIGURE 19. (a), (b). Fabricated design top view and bottom view respectively, (c) fabricated design in anechoic chamber measurement facility.

TABLE 4. Simulated and measured ECC and DG.

Sr. No	Frequency (GHz)	ECC (Simulated)	ECC (Measured)	DG (Simulated)	DG (Measured)
1	2.85	< 0.02	0.05	9.99	9.5
2	4.44	< 0.02	0.02	9.99	9.99
3	5.81	< 0.02	0.03	9.99	9.80
4	6.46	< 0.02	0.02	9.99	9.99
5	7.02	< 0.02	0.02	9.99	9.99

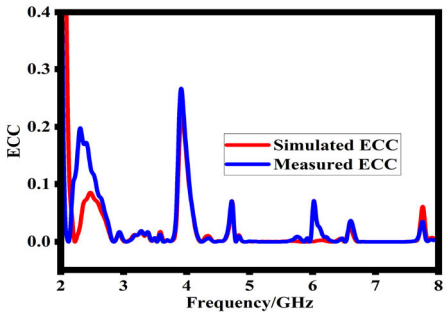

FIGURE 20. ECC of the proposed MIMO design.

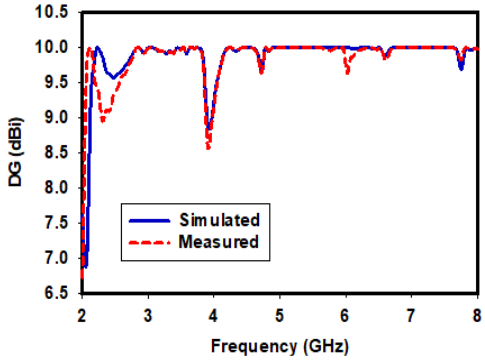

FIGURE 21. Diversity Gain of the proposed MIMO design.

D. TOTAL ACTIVE REFLECTION COEFFICIENT (TARC)

Total active reflection coefficient is an important parameter used to analyze MIMO antenna systems performance. It gives detail of the total reflection of the active power at the transmitting and receiving antennas ports. It also defines the total effective bandwidth of the antennas. Equation (20) is used to determine the TARC of the proposed design [26].

$$\text{TARC} = N^{-0.5} * \sqrt{\sum_{i=1}^{N} \left| \sum_{k=i}^{N} s_{ik} e^{j\theta_{k-1}} \right|^2} \tag{20}$$

A TARC of 0 db is considered an acceptable value for the effective communication. Any value better than this further strengthen the effectiveness of TARC for the proposed design. Figure 23 shows that the proposed design has achieved the values of TARC better than 15 db at all resonance frequencies.

Table 5 provides a thorough comparison of the aimed research with previously published studies. A number of important factors are compared, including electrical and physical dimensions, the number of working bands, maximum gain, envelope correlation coefficient (ECC), and diversity gain (DG). From the comparison, it is evident that the proposed work offers a compact size while delivering impressive performance characteristics. The antenna design achieves a smaller electrical and physical size compared to the published studies, indicating its potential for space-constrained applications. Moreover, the proposed design

TABLE 5. Comparison of the proposed work with the state of the art.

Ref. No	Size (λ^3)	Size (mm^3)	Bands (GHz)	Max Gain (dBi)	ECC	Diversity Gain [dB]
[26]	0.373 × 0.373 × 0.093	90 × 90 × 1	2	N/A	0.007	9.98
[28]	0.264 × 0.264 × 0.120	100 × 100 × 20	3	6.9	< 0.2	≅ 10
[29]	0.220 × 0.132 × 0.073	37.× 37.6 × 5	3	5.7	0.003	9.98
[30]	Not given	80 × 80 × 6.5	2	N/A	0.25	Not Given
[31]	0.087 × 0.087 × 0.034	90 × 107.8 × 11.4	3	3.7	0.005, 0.003, 0.0064	10, 9.9999, 9.9997
[32]	0.3 × 0.058 × 0.194	110 × 50 × 16.5	2	6.8	< 0.5	> 9.8
Proposed Work	0.093 × 0.093 × 0.046	40 × 80 × 5	5	6.08	0.004, 0.0001, 0.0019, 0.0003, 0.0001	9.9980, 9.9997, 9.9915, 9.9979, 9.9999

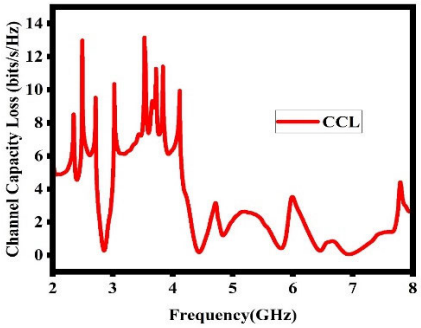

FIGURE 22. Channel capacity loss of the proposed design at the operating bands.

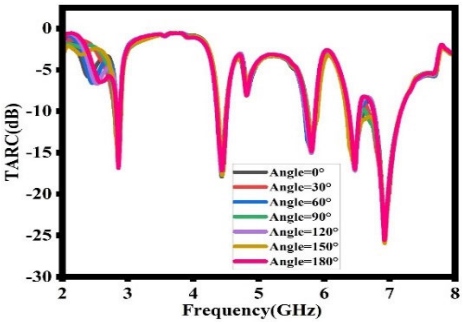

FIGURE 23. TARC of the proposed design at five operating bands.

demonstrates a comparable or superior number of operating bands, maximum gain, ECC, and DG when compared to the referenced works. This highlights the effectiveness and competitiveness of the proposed antenna design in terms of size, performance, and MIMO capabilities over 20 dB isolation. The fabricated prototype aligns closely with the simulated results, confirming the suitability and and introducing an air gap. Moreover, the inclusion of an inverted T-shaped slot in the ground plane has significantly improved mutual impedance, leading to enhanced isolation between the MIMO elements. The MIMO DRA exhibited impressive diversity parameters, including a maximum diversity gain of 10 dB and an envelope correlation coefficient of 0.005 over 20 dB isolation. The fabricated prototype aligns closely with the simulated results, confirming the suitability and reliability of the CSRR-based MIMO DRA design. With its compact size, high performance, and the provision of five operating bands, the proposed design holds promise for various wireless applications.

VI. CONCLUSION

A compact MIMO DRA based on CSRRs and an inverted T-shaped slot has been successfully designed, simulated, fabricated and tested. The proposed MIMO DRA demonstrates excellent performance characteristics and versatility for multiband wireless applications. Through the integration of CSRRs, the MIMO DRA achieves resonance at five distinct frequency bands, namely 2.8 GHz, 4.4 GHz, 5.8 GHz, 6.4 GHz, and 6.9 GHz, offering a wide range of operating frequencies. The impedance matching has been effectively enhanced by incorporating a printed strip to the DR and introducing an air gap. Moreover, the inclusion of an inverted T-shaped slot in the ground plane has significantly improved mutual impedance, leading to enhanced isolation between the MIMO elements. The MIMO DRA exhibited impressive diversity parameters, including a maximum diversity gain of 10 dB and an envelope correlation coefficient of 0.005 over 20 dB isolation. The fabricated prototype aligns closely with the simulated results, confirming the suitability and reliability of the CSRR-based MIMO DRA design. With its compact size, high performance, and the provision of five operating bands, the proposed design holds promise for various wireless applications.

REFERENCES

[1] A. Mahesh, K. S. Shushrutha, and R. K. Shukla, "Design of multi-band antennas for wireless communication applications," in *Proc. IEEE Appl. Electromagn. Conf. (AEMC)*, Dec. 2017, pp. 1–2.

[2] R. D. Darawade, A. S. Kothari, S. V. Edhate, R. K. Vipul, and C. M. Prashant, "A review on dielectric resonator antenna and its analysis setup," *Int. J. Sci. Res. Sci. Eng. Technol.*, vol. 4, no. 7, pp. 282–289, 2018.

[3] S. Keyrouz and D. Caratelli, "Dielectric resonator antennas: Basic concepts, design guidelines, and recent developments at millimeter-wave frequencies," *Int. J. Antennas Propag.*, vol. 2016, pp. 1–20, Jan. 2016.

[4] I. Ali, M. H. Jamaluddin, A. Gaya, and H. A. Rahim, "A dielectric resonator antenna with enhanced gain and bandwidth for 5G applications," *Sensors*, vol. 20, no. 3, p. 675, Jan. 2020.

[5] D. Batra, S. Sharma, and A. K. Kohli, "Dual-band dielectric resonator antenna for C and X band application," *Int. J. Antennas Propag.*, vol. 2012, Apr. 2012, Art. no. 914201.

[6] P. Zenita, G. Kumar, and R. Malik, "Dielectric resonator antenna for MIMO applications: A review," *Int. J. Sci. Eng. Technol.*, vol. 8, no. 4, pp. 2–6, 2020.

[7] K. Wa Leung, "Conformal strip excitation of dielectric resonator antenna," *IEEE Trans. Antennas Propag.*, vol. 48, no. 6, pp. 961–967, Jun. 2000.

[8] I. Ali, M. H. Jamaluddin, and A. Gaya, "Higher order mode dielectric resonator antenna excited using microstrip line," *Bull. Electr. Eng. Informat.*, vol. 9, no. 4, pp. 1734–1738, Aug. 2020.

[9] D. Gharode, A. Nella, and M. Rajagopal, "State-of-art design aspects of wearable, mobile, and flexible antennas for modern communication wireless systems," *Int. J. Commun. Syst.*, vol. 34, no. 15, Oct. 2021.

[10] S. E. Mendhe and Y. P. Kosta, "Metamaterial properties and applications," *Int. J. Inf. Technol. Knowl. Manag.*, vol. 4, no. 1, pp. 85–89, 2011.

[11] W. J. Krzysztofik, "Antenna properties improvement by means of modern technology," in *Proc. 20th Int. Conf. Microw., Radar Wireless Commun. (MIKON)*, Jun. 2014, pp. 1–4.

[12] W. J. Krzysztofik, "Fractals in antennas and metamaterials applications," in *Fractal Analysis—Applications in Physics, Engineering and Technology*, InTech, Jun. 2017.

[13] W. J. Krzysztofik and T. N. Cao, "Metamaterials in application to improve antenna parameters," in *Metamaterials and Metasurfaces*. London, U.K.: IntechOpen, Jan. 2019.

[14] M. Ramzan and K. Topalli, "A miniaturized patch antenna by using a CSRR loading plane," *Int. J. Antennas Propag.*, vol. 2015, pp. 1–9, Jul. 2015.

[15] A. El Yousfi, A. Lamkaddem, K. A. Abdalmalak, and D. Segovia-Vargas, "A miniaturized triple-band and dual-polarized monopole antenna based on a CSRR perturbed ground plane," *IEEE Access*, vol. 9, pp. 164292–164299, 2021.

[16] D. Pal, R. Singhal, A. Joshi, and A. K. Bandyopadhyay, "Multiband planar antenna with CSRR loaded ground plane for WLAN and fixed satellite service applications," *Frequenz*, vol. 74, nos. 11–12, pp. 393–399, Nov. 2020.

[17] V. Sharma, S. Yadav, and K. R. Saraswat, "SRR inspired multiband antenna for wireless applications," *Int. J. Eng. Res. Technol.*, vol. 8, vol. 3, pp. 10–12, Mar. 2019.

[18] R. Xie, J. Cao, and S. Zhu, "A compact multi-band dielectric resonator antenna loaded with CSRRs for communication systems," in *Proc. 10th Int. Congr. Adv. Electromagn. Mater. Microw. Opt. (METAMATERIALS)*, Sep. 2016, pp. 421–423.

[19] N. Embong and M. F. Mansor, "Multiband dielectric resonator antenna (DRA) for long term evolution advanced (LTE—A) handheld devices," in *Proc. Int. Conf. Space Sci. Commun. (IconSpace)*, Aug. 2015, pp. 38–41.

[20] S. Mani and L. Edeswaran, "High gain multiband stacked DRA for Wimax and WLAN applications," *Amer. J. Appl. Sci.*, vol. 14, no. 8, pp. 779–785, Aug. 2017.

[21] A. Buerkle, K. Sarabandi, and H. Mosallaei, "Compact slot and dielectric resonator antenna with dual-resonance, broadband characteristics," *IEEE Trans. Antennas Propag.*, vol. 53, no. 3, pp. 1020–1027, Mar. 2005.

[22] Y.-F. Lin, H.-M. Chen, and C.-H. Lin, "Compact dual-band hybrid dielectric resonator antenna with radiating slot," *IEEE Antennas Wireless Propag. Lett.*, vol. 8, pp. 6–9, 2009.

[23] R. Khan, M. H. Jamaluddin, J. U. R. Kazim, J. Nasir, and O. Owais, "Multiband-dielectric resonator antenna for LTE application," *IET Microw., Antennas Propag.*, vol. 10, no. 6, pp. 595–598, Apr. 2016.

[24] P. R. Girjashankar and T. K. Upadhyaya, "Surface mountable multi-band DRA for wireless communication systems," *PIER J.*, vol. 103, pp. 173–183, Jul. 2021.

[25] K. Ishimiya, J. Langbacka, Z. Ying, and J. Takada, "A compact MIMO DRA antenna," in *Proc. Int. Workshop Antenna Technol., Small Antennas Novel Metamaterials*, Mar. 2008, pp. 286–289.

[26] M. D. Alanazi and S. K. Khamas, "A compact dual band MIMO dielectric resonator antenna with improved performance for mm-wave applications," *Sensors*, vol. 22, no. 13, p. 5056, Jul. 2022.

[27] V. Kumar, "Rectangular DR-based dual-band CP-MIMO antenna with inverted Z-shaped slot," *Int. J. Electron.*, vol. 107, no. 10, pp. 1559–1573, Oct. 2020.

[28] S. U. Anuar, M. H. Jamaluddin, J. Din, K. Kamardin, M. H. Dahri, and I. H. Idris, "Triple band MIMO dielectric resonator antenna for LTE applications," *AEU Int. J. Electron. Commun.*, vol. 118, May 2020, Art. no. 153172.

[29] S. K. Yadav, A. Kaur, and R. Khanna, "Compact cross-shaped parasitic strip based multiple-input multiple-output (MIMO) dielectric resonator antenna for ultra-wideband (UWB) applications," *Frequenz*, vol. 75, nos. 5–6, pp. 191–199, May 2021.

[30] G. Das, A. Sharma, R. K. Gangwar, and M. S. Sharawi, "Compact back-to-back DRA-based four-port MIMO antenna system with bi-directional diversity," *Electron. Lett.*, vol. 54, no. 14, pp. 884–886, Jul. 2018.

[31] I. K. C. Lin, M. H. Jamaluddin, A. Awang, R. Selvaraju, M. H. Dahri, L. C. Yen, and H. A. Rahim, "A triple band hybrid MIMO rectangular dielectric resonator antenna for LTE applications," *IEEE Access*, vol. 7, pp. 122900–122913, 2019.

[32] S. S. Singhwal, B. K. Kanaujia, A. Singh, J. Kishor, and L. Matekovits, "Dual-band circularly polarized MIMO DRA for sub-6 GHz applications," *Int. J. RF Microw. Comput. Aided Eng.*, vol. 30, no. 10, pp. 1–12, Oct. 2020.

[33] G. Das, A. Sharma, and R. K. Gangwar, "Dielectric resonator-based two-element MIMO antenna system with dual band characteristics," *IET Microw., Antennas Propag.*, vol. 12, no. 5, pp. 734–741, Apr. 2018.

[34] A. Sharma, G. Das, and R. K. Gangwar, "Design and analysis of tri-band dual-port dielectric resonator based hybrid antenna for WLAN/WiMAX applications," *IET Microw., Antennas Propag.*, vol. 12, no. 6, pp. 986–992, May 2018.

[35] K. Li, Y. Shi, and C. Liang, "Quad-element multi-band antenna array in the smart mobile phone for LTE MIMO operations," *Microw. Opt. Technol. Lett.*, vol. 58, no. 11, pp. 2619–2626, Nov. 2016.

[36] H. A. Malhat and S. H. Zainud-Deen, "Low-profile quad-band perforated rectangular dielectric resonator antenna for wireless communications," *J. Eng.*, vol. 2017, no. 8, pp. 448–451, Aug. 2017.

[37] S. Zhang, B. K. Lau, Y. Tan, Z. Ying, and S. He, "Mutual coupling reduction of two PIFAs with a T-shape slot impedance transformer for MIMO mobile terminals," *IEEE Trans. Antennas Propag.*, vol. 60, no. 3, pp. 1521–1531, Mar. 2012.

HARRIS SARFRAZ received the B.Sc. and M.Sc. degrees in electrical engineering from COMSATS University Islamabad, Abbottabad Campus, Pakistan. He is an accomplished Electrical Engineer in Pakistan. With a strong commitment to advancing antenna technology, he aims to develop innovative solutions for improved wireless communication systems. He is determined to explore new frontiers and address the challenges faced by wireless communication systems. He aims to contribute to the development of innovative and efficient antenna solutions that can enhance the performance and reliability of modern wireless networks. His research interests include several cutting-edge topics, including dielectric resonator antennas, multiband antennas, mimo antennas, and metamaterials.

SHAHID KHAN was born in Landi Kotal, Pakistan, in 1986. He received the B.S. degree in telecommunication engineering from the University of Engineering and Technology, Peshawar, Pakistan, the M.S. degree in satellite navigation and related applications from Politecnico de Torino, Italy, in 2011, and the Ph.D. degree from the University of Lorraine, France, in 2021. He was a Visiting Fellow with the 5G Innovation Center, University of Surrey. He is currently an Assistant Professor with the Department of Electrical and Computer Engineering, COMSATS University Islamabad, Abbottabad Campus. He is working on the development of circularly polarized phased array DRAs for satellite applications, implantable antennas, and reconfigurable dielectric resonator antennae for different wireless applications.

NASEER KHAN received the B.Sc. degree in electrical engineering from the University of Engineering and Technology, Peshawar, Pakistan, in December 2007. Since then, he has been a Lecturer with COMSATS University Islamabad, Abbottabad Campus, where he teaches and conducts research in the field of electronic device design for wireless communication and its applications in microchips. His research interests include exploring new technologies and techniques for improving the efficiency and performance of electronic systems.

NEELAM GOHAR received the Ph.D. degree from the University of Liverpool, U.K., in 2012. She has been the Head of the Department of Computer Science, Shaheed Benazir Bhutto Women University, Peshawar, Pakistan, for more than eight years. She is also an Assistant Professor. She participated in national and international training programs. She has published more than 15 articles in an international impact factor peer-reviewed journals. Her research interests include wireless communication, artificial intelligence, multi-agent systems, computational social choice theory, algorithmic game theory, data analytics, and data science. She is a reviewer of different journals and international conferences, organized national and international conferences, and academic events, and resource person for different trainings, a member of different committees, such as the establishment of smart classrooms and community college, a technical member of online readiness committee and postgraduate review committee, a focal person of different projects of HEC, a member of national curriculum revision committee in the field of IT, software engineering, and computer science, recognized as an IT Professional by the Information and Communication Technology Council (ICTC), Canada.

SYED AHSON ALI SHAH (Member, IEEE) received the B.Sc. degree in telecommunication engineering from the University of Engineering and Technology, Mardan, Pakistan, in 2015, and the M.S. leading to Ph.D. degree in electronic engineering from the Applied Bioelectronics Laboratory, Hanyang University, Seoul, South Korea, in 2022, under the supervision of Dr. Hyoungsuk Yoo. From September 2022 to March 2023, he was a Postdoctoral Researcher with the Applied Bioelectronics Laboratory, Hanyang University. Since April 2023, he has been a Postdoctoral Researcher with the Mobile Power Electronics Laboratory and the Power Systems Laboratory, Gwangju Institute of Science and Technology, Gwangju, South Korea. To date, he has published several journal articles and conference papers. His research interests include free-space antennas for wireless communications, implantable antennas and systems, implant safety, wireless power transfer systems, sensor-integrated biotelemetric stents, reconfigurable antennae, metamaterial-based antenna systems, and 5G antenna developments. He received the IETE MN SAHA Memorial Award and the Gold Medal for Best Application-Oriented Paper, in 2018. He also received the Bronze Paper Award from the IEEE Student Paper Contest, Seoul, in 2019, 2021, and 2022. He also Won the Third Best Student Paper Award, in 2021, a Competition arranged by the Korean Institute of Electromagnetic Engineering and Science (KIEES). His Ph.D. thesis has been recognized as one of the Excellent Dissertations and received the Best Ph.D. Thesis Award in overall university and the only one in the Electronic Engineering Department. He has been a Registered Engineer with the Pakistan Engineering Council (PEC), Pakistan, since 2016. He is also serving as a Reviewer for IEEE TRANSACTIONS ON ANTENNAS AND PROPAGATION, IEEE TRANSACTIONS ON INDUSTRIAL ELECTRONICS, IEEE ACCESS, the *International Journal of RF and Microwave Computer-Aided Engineering*, and *SN Applied Sciences*.

JAMAL NASIR was born in Malakand Agency, Khyber Pakhtunkhwa, Pakistan, in 1983. He received the M.Sc. degree in mobile and satellite communication from the University of Bradford, U.K., in 2007, and the Ph.D. degree in electrical engineering from Universiti Teknologi Malaysia, in 2017. He is currently an Assistant Professor with the Department of Electrical Engineering, COMSATS University Islamabad, Abbottabad Campus, Khyber Pakhtunkhwa. His research interests include SIW-based passive components and arrays, metamaterials, smart antennas, mutual coupling analysis, MIMO antennas, dielectric resonator antennas, UWB antennas, slotted waveguide arrays, ingestible and implantable antennas, and wearable antennas.

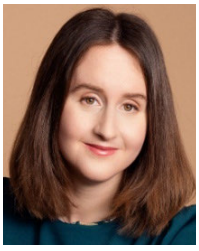

MARIANA DALARSSON (Senior Member, IEEE) received the M.Sc. degree in physics and the Ph.D. degree in electromagnetic theory from the KTH Royal Institute of Technology, Stockholm, Sweden, in 2010 and 2016, respectively, and the Docent degree from Linnaeus University, Växjö, Sweden, in 2019. From 2016 to 2019, she was a Postdoctoral Researcher with the Group of Waves, Signals and Systems, Linnaeus University. From 2019 to 2010, she was an Assistant Professor with the Department of Electrical and Information Technology, Lund University, Lund, Sweden. She is currently an Assistant Professor with the KTH Royal Institute of Technology. She is the author of more than 80 scientific publications, including 40 journal articles, and one book. She is mainly pursuing research as a PI within her project grant "Waveguide Theory for Artificial Materials and Plasmonics" awarded by the Swedish Research Council. Her teaching and research interests include antenna theory, electromagnetic scattering and absorption, inverse problems, electromagnetics of stratified media, double-negative metamaterials, and mathematical physics. She is the Second Youngest Woman ever to be awarded the Ph.D. degree from the KTH Royal Institute of Technology. She received the Honorary Grant given to the Best Graduate of the Year of the M.Sc. Program, in 2011. She is the Winner of multiple teaching and research awards, including the L'Oréal-UNESCO For Women in Science Sweden Awards, in 2021.